DLR
German Aerospace Center

# ANALYSIS OF NUCLEAR MORPHOLOGY OF DESMIN KNOCK-OUT MYOBLASTS


Bachelor thesis

Submitted by

Elena Anna-Maria Honscheid

Cologne, July 2020

This study was conducted from May to July 2020 at the Institute of Aerospace-Medicin, German Aerospace Center, Cologne, in the work group “Molecular Muscle and Bone Research” under the supervision of Prof. Dr. med. Christoph S. Clemen.

**1st supervisor:** Prof. Dr. rer. nat. Jan Riemer
Institute of Biochemistry
University of Cologne

**2nd supervisor:** Prof. Dr. rer. nat. Ines Neundorf
Institute of Biochemistry
University of Cologne

**Eidesstattliche Erklärung**

Hiermit versichere ich an Eides statt, dass ich die vorliegende Arbeit selbstständig und ohne die Benutzung anderer als der angegebenen Hilfsmittel angefertigt habe.
Alle Stellen, die wörtlich oder sinngemäß aus veröffentlichten und nicht veröffentlichten Schriften entnommen wurden, sind als solche kenntlich gemacht.
Die Arbeit ist in gleicher oder ähnlicher Form oder auszugsweise im Rahmen einer anderen Prüfung noch nicht vorgelegt worden.
Ich versichere, dass die eingereichte elektronische Fassung der eingereichten Druckfassung vollständig entspricht.

Ich bin mir bewusst, dass die falsche Abgabe der Versicherung an Eides statt die Rechtsfolgen des § 63 Absatz 5 HG Anwendung finden.

**Köln, 27.07.2020**
Ort, Datum


Unterschrift

# TABLE OF CONTENT

# ABSTRACT

Desminopathies are degenerative muscle diseases caused by mutations of the desmin gene. Desmin is an intermediate filament protein that is mainly expressed in smooth muscles, skeletal muscles and cardiac muscles cells. There it connects the nuclei, mitochondria, myofibrils, and the sarcolemma, thus providing the structure within the cells. Mutations of the desmin gene lead to autosomal-dominant, autosomal recessive and sporadic myopathies and/or cardiomyopathies (Clemen, Herrmann et al. 2013). Recessive forms of the disease include the complete absence of desmin (Henderson, De Waele et al. 2013, Ruppert, Heckmann et al. 2020). To investigate this form of the disease in more detail, desmin knock-out mice were already bred. This study is mainly concerned with the nuclear morphology of the myoblasts (muscle precursor cells), of the mice mentioned above. In cardiomyocytes it has already been observed that a knock-down of desmin led to misfolded nuclei (Heffler, Shah et al. 2020).

To investigate the issue in skeletal muscle derived cells, murine wild-type myoblasts were compared with homozygous desmin knock-out myoblasts. First, it was determined whether the newly generated myoblast cells lines are suitable for further experiments by testing their growth and differentiation ability. Afterwards, several immunofluorescence stainings were performed, which stained the inner or outer nuclear envelope or the nuclear lamina. In addition, the myoblasts were exposed to lower oxygen conditions to observe oxygen-dependent changes of the nuclear morphology.

The immunofluorescence images of the homozygous desmin knock-out myoblasts also showed crumpled or folded nuclei, and also a significant decrease in nuclear size. When the myoblasts were exposed to an oxygen concentration of 1%, fewer nuclear abnormalities were observed in homozygous cells, while the number of abnormalities in wild-type cells remained unchanged. Moreover, the nuclei of myoblasts exposed to 1 % were significantly larger in both wild-type and homozygous desmin knock-out myoblasts as compared to 21% oxygen. Since Desmin is connected to the nuclear envelope via components of the LINC complex, these findings may indicate that desmin has a traction function that supports the nucleus in its oval or round shape (Heffler, Shah et al. 2020).

Furthermore, a comparison of wild-type and desmin knock-out nuclei of cultured myoblasts and mature muscle tissue revealed similarly smaller nuclei, which verifies the myoblasts cell lines as valuable model system.

## ZUSAMMENFASSUNG

Desminopathien sind degenerative Muskelkrankheiten, die durch Mutationen des Desmin-Gens verursacht werden. Desmin ist ein Intermediär Filament Protein, das hauptsächlich in glatten Muskel-, Skelettmuskel- und Herzmuskelzellen exprimiert wird. Dort verbindet es den Zellkern, die Mitochondrien, Myofibrillen und dem Sarkolemm und bildet so die Struktur innerhalb der Zellen. Mutationen des Desmin Gens führen zu autosomal-dominanten, autosomal-rezessiven und sporadischen Myopathien und/oder Kardiomyopathien (Clemen, Herrmann et al. 2013). Zu den rezessiven Formen der Erkrankung gehört das vollständige Fehlen von Desmin (Henderson, De Waele et al. 2013, Ruppert, Heckmann et al. 2020). Um diese Form der Erkrankung näher zu untersuchen, wurden bereits Desmin-Knock-out-Mäuse gezüchtet. Diese Studie befasst sich hauptsächlich mit der Kernmorphologie der Myoblasten (Muskelvorläuferzellen) der oben erwähnten Mäuse. In Kardiomyozyten wurde bereits beobachtet, dass ein Knock-down von Desmin zu falsch gefalteten Kernen führt (Heffler, Shah et al. 2020).

Um dieses Problem in Skelettmuskelzellen zu untersuchen, wurden die murinen Wildtyp Myoblasten mit homozygoten Desmin-Knock-out-Myoblasten verglichen. Zunächst wurde festgestellt, ob die neu erzeugten Myoblastenzelllinien für weitere Experimente geeignet waren, indem ihre Wachstums- und Differenzierungsfähigkeit getestet wurde. Danach wurden mehrere Immunfluoreszenz-Färbungen durchgeführt, bei denen die innere oder äußere Kernhülle oder auch die Kernlamina angefärbt wurden. Darüber hinaus wurden die Myoblasten bei niedrigeren Sauerstoffkonzentrationen ausgesetzt, um sauerstoffabhängige Veränderungen der Kernmorphologie zu beobachten.

Die Immunfluoreszenzbilder der homozygoten Desmin Knock-out-Zellen zeigten ebenfalls zerknitterte oder gefaltete Kerne, und auch eine signifikante Abnahme der Kerngröße. Wurden die Myoblasten einer Sauerstoffkonzentration von 1 % ausgesetzt, wurden weniger nukleäre Anomalien bei den homozygoten Desmin Knock-out Myoblasten beobachtet, die Zahl der Anomalien bei Wildtyp Myoblasten blieb unverändert. Darüber hinaus waren die Kerne sowohl beim Wildtyp als auch bei den homozygoten Knock-out-Myoblasten signifikant größer als bei 21% Sauerstoff. Da Desmin über Komponenten des LINC Komplexes mit der Zellkernhülle verbunden ist, können diese Daten darauf hinweisen, dass Desmin eine Zugfunktion hat, die den Kern in seiner ovalen oder runden Form unterstützt (Heffler, Shah et al. 2020).

Außerdem ergab ein Vergleich von Wildtyp- und Desmin-Knock-out-Kernen von kultivierten Myoblasten und reifem Muskelgewebe ähnlich kleinere Kerne, was die Myoblasten-Zelllinien als wertvolles Modellsystem verifiziert.

# 1 INTRODUCTION

## 1.1 CYTOSKELETON

The cytoskeleton is an intracellular protein network giving animal cells structure and shape (Christen, Jaussi et al. 2016) and it is also a necessary component for the stability of the cells (Herrmann, Bar et al. 2007). Furthermore, it is important for the organization and positioning of cell organelles and intracellular movement by motor proteins. The cytoskeleton proteins are categorized into three major groups: actin filaments, intermediate filaments, and microtubules (Christen, Jaussi et al. 2016). In contrast to plant cells, animal cells do not have cell walls handle mechanical stress. To resist pressure and tension, animal cells are in need of a stronger intracellular cytoskeleton than plant cells (Herrmann, Bar et al. 2007).

## 1.2 INTERMEDIATE FILAMENTS

Intermediate filaments (IFs) are a group of the cytoskeleton protein family. They are cord-like, fibrous, polymerized proteins, mainly expressed in cells that are exposed to mechanical stress (Herrmann, Bar et al. 2007, Christen, Jaussi et al. 2016). Compared to actin filaments and microtubules, intermediate filaments are highly elastic and tear-resistant. Since plant cells require less mechanical support, intermediate filament proteins are much less expressed. (Christen, Jaussi et al. 2016). Lamins forming the nuclear lamina, belong to the intermediate filament protein family as well. Through a linking complex (LINC complex) the nuclear lamina is connected to the cytoplasmic intermediate filament cytoskeleton, which spreads out throughout the entire cell (Christen, Jaussi et al. 2016).

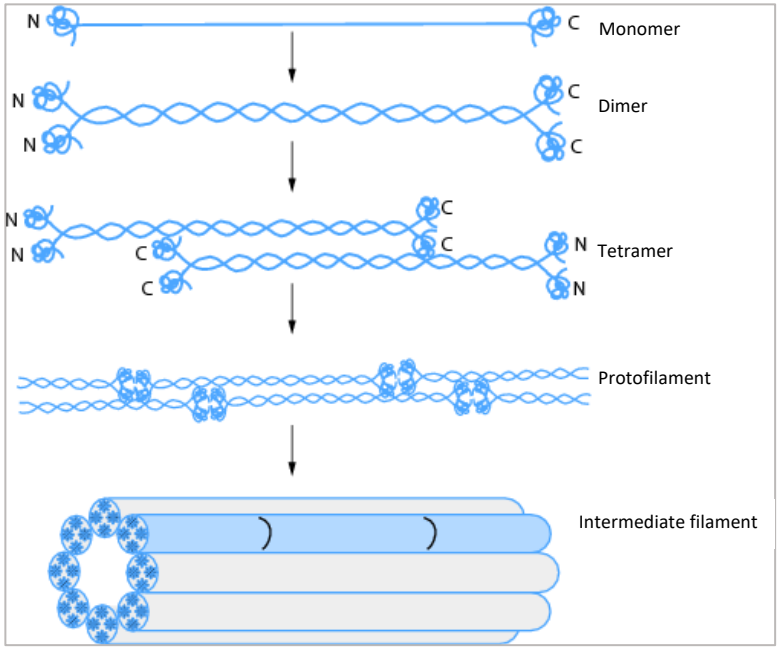


***Figure 1. Assembly process of intermediate filament**. Monomers form coiled-coil dimers, which assemble to tetramers. Multiple tetramers form the protofilaments, which assemble into mature intermediate filament (Boujard, Anselme et al. 2014)*

Different kinds of intermediate filament proteins are expressed in different cell types and their expression also varies between embryogenesis and differentiation (Herrmann, Bar et al. 2007). During the assembly process of an intermediate filament two monomers form a coiled-coil dimer in parallel orientation. Those dimers assemble to antiparallel and slightly displaced tetramers, which spontaneously build protofilaments (Herrmann, Strelkov et al. 2009, Boujard, Anselme et al. 2014). These protofilaments assemble into mature intermediate filaments (figure 1).

## 1.3 DESMIN

Desmin is a 470 amino-acid long protein (Herrmann, Strelkov et al. 2009) encoded by the desmin gene (DES) on human chromosome 2q35 (Li, Lilienbaum et al. 1989). It belongs to the intermediate filament protein family and is mainly expressed in skeletal muscle, cardiac muscle and smooth muscle cells. In the muscle cells, desmin filaments connect myofibrils, mitochondria, nuclei and the sarcolemma (Schröder and Schoser 2009). Desmin is essential for the correct orientation and alignment of myofibrils as well as the positioning of mitochondria and nuclei within muscle cells. It therefore plays important roles in both structure, function and signal pathways due to mechanical force transmission (Clemen, Herrmann et al. 2013).

## 1.4 DESMINOPATHIES and MYOFIBRILLAR MYOPATHIES

The desmin gene is 8.6 kb long single copy gene, containing 9 exons (Li, Lilienbaum et al. 1989). Multiple mutations of the human desmin gene have been documented that cause diseases so-called desminopathies (Clemen, Herrmann et al. 2013, Hnia, Ramspacher et al. 2015). Desminopathies are genetical skeletal muscle diseases that belong to the myofibrillar myopathies, i.e. diseases with degenerative changes of the myofibrils within the muscle cell. Myofibrillar myopathies can be caused by mutations of myofibrillar proteins as well as extramyofibrillar proteins such as desmin (Schröder and Schoser 2009). The mutations are autosomal-dominantly or recessively inherited or occur sporadically (Clemen, Herrmann et al. 2013). Like neurodegenerative diseases such as Parkinson's, myofibrillary myopathies are associated with pathological protein aggregations. In the case of desminopathies, mutant desmin causes desmin-positive protein aggregates in the cytoplasm as well as pathological changes in myofibrils. These changes finally lead to muscle weakness, which in the

case of a "classical" desminopathy mainly affects the lower extremities (Schröder and Schoser 2009), but also to cardiac involvements like dilatation (Milner, Weitzer et al. 1996) and arrhythmias (Milner, Taffet et al. 1999). Desminopathies can manifest itself in the first to eighth decade of life as cardiomyopathy, myopathy, or both combined (Clemen, Herrmann et al. 2013). Premature death is usually caused by sudden cardiac death, progressive heart failure or respiratory insufficiency (van Spaendonck-Zwarts, van Hessem et al. 2011, Clemen, Herrmann et al. 2013).

### *1.4.1 DESMIN KNOCK-OUT PATIENTS*

Certain forms of the very rare autosomal-recessive desminopathies can result in the complete absence of desmin. However, the clinical picture of these patients differs from the more common autosomal-dominant forms and may not immediately recognizable as such (Henderson, De Waele et al. 2013). But these forms show a more severe progression and an earlier manifestation of the disease (Ruppert, Heckmann et al. 2020).

## 1.5 DESMIN KNOCK-OUT MICE

To better understand the function of desmin, desmin knock-out mice were independently generated by two different research groups (Li, Colucci-Guyon et al. 1996, Milner, Weitzer et al. 1996). Desmin knock-out mice developed progressive myopathies and cardiomyopathies. In the skeletal muscles, unorganized and unaligned myofibers were observed (Li, Colucci-Guyon et al. 1996). Injection with AVV9 vectors containing the desmin cDNA led to a re-expression of desmin followed by a normalization of the heart function and a regular distribution of desmin within cardiomyocytes (Ruppert, Heckmann et al. 2020).

## 1.6 DESMIN KNOCK-DOWN IN CARDIOMYOCYTES

A recent study by Heffler et al. (2020) investigated the relevance of desmin in cardiomyocytes and its effects on the shape of the myonuclei. Knock-downs (KD) of desmin and nesprin-3, a nuclear envelope protein and part of the LINC complex that binds desmin to the nuclear lamina, were therefore performed. The result was a decrease in nuclear volume, height and width but an increase in nuclear length. Further, multiple infoldings in the nuclei of both desmin and nesprin-3 knock-down cardiomyocytes were observed. The knock-down of desmin thought to lead to a lack of tension on the nuclear envelope, so that

the longitudinal axis of the nuclei is dented by microtubules (Heffler, Shah et al. 2020). Additionally, they discovered that the desmin knock-down caused DNA damages in form of double-stranded breaks possibly due to the folding shape of the nuclei (Heffler, Shah et al. 2020).

## 1.7 MYOBLASTS and MYOGENESIS

The origin of mammalian skeletal musculature is the mesoderm. During embryogenesis, the myogenic precursor cells that emerge from the mesoderm differentiate into myoblasts. These myoblasts proliferate and differentiate further. They then fuse with other myoblasts to form a syncytium, an elongated multinuclear myotube (Boujard, Anselme et al. 2014, Beaudry, Hidalgo et al. 2016, Chal and Pourquie 2017). These myotubes subsequently mature into muscle fibers. The cytoplasm of the muscle fibers (sarcoplasm) contains mainly myofibrils, which consist of the contractile elements (sarcomeres). The special order of the myofibrils within the fibers, so that the sarcomeres are arranged in parallel, results in the striated pattern typical for striated muscles (Boujard, Anselme et al. 2014).

In addition, mammalian skeletal muscles are capable of growth and are to a certain extent able to recover from damage by exercise or disease. Therefore, stem cells are present in the muscle, so-called satellite cells (Boujard, Anselme et al. 2014). Satellite cells have the same origin like myoblasts and are placed between the basal lamina, enveloping the muscle fiber, and it's sarcolemma (Gros, Manceau et al. 2005). Since these cells do not have a connection to blood vessels, satellite cells live in hypoxic microenvironment (Beaudry, Hidalgo et al. 2016). Satellite cells proliferate and form myoblasts, which similar to embryonic muscle development determine to myotubes and then into mature muscle fibers (Li, Zhu et al. 2007, Beaudry, Hidalgo et al. 2016).

The different stages of myogenesis are characterized by the expression of specific transcription factors. The pair-box proteins Pax3 and Pax7 (Relaix, Rocancourt et al. 2005) and the myogenic factors Myf5 (Ott, Lyons et al. 1991) and MyoD (Wright, Sassoon et al. 1989) are detectable in proliferating myoblasts and also necessary for skeletal muscle cell fate (Kassar-Duchossoy, Gayraud-Morel et al. 2004). During determination into myotubes Pax3 and Pax7 are decreased and myogenic factors such as myogenin (Wright, Sassoon et al. 1989) are expressed additionally to MyoD and Myf5 (Chal and Pourquie 2017).

## 1.8 NUCLEAR MORPHOLOGY

The nuclear shape can vary greatly depending on the cell type and also between species (Skinner and Johnson 2017). For instance, cells of the immune system often have lobed or multi-lobed nuclei (Hoffmann, Sperling et al. 2007), while myoblast nuclei are usually ovoid (Abe, Takano et al. 2004). Nuclear size often correlated with the size of the cell. Smaller cells usually have smaller nuclei (Huber and Gerace 2007).

There are many factors that influence nuclear morphology, including cell function and environment, cytoskeletal connections, but also diseases (Skinner and Johnson 2017).

The nuclear envelope consists of an inner and an outer nuclear membrane, separating the DNA from the cytoplasm (Hetzer 2010). Underneath the inner membrane lies the nuclear lamina, a nuclear cytoskeleton network consisting of the proteins lamin A, B and C. The nuclear lamina provides the nucleus with additional stability (Boujard, Anselme et al. 2014). It is assumed, that the cytoskeleton via the LINC complex and the nuclear lamina has a deep impact on nuclear shape (Skinner and Johnson 2017).

## 1.9 LINC COMPLEX

The nuclear envelope is permeated by a complex structure that connects the nucleoskeleton and the cytoskeleton, the so-called LINC complex (figure 2). The functions of this complex are manifold including cell signaling, meiosis or DNA damage repair (Cartwright and Karakesisoglou 2014). Mechanical forces can be directly transmitted by the cytoskeleton to the nucleus and can change gene expression (Skinner and Johnson 2017). The sun and nesprin proteins are the important connecting proteins in this complex, they form a “nuclear envelope bridge” (Starr and Fridolfsson 2010). Nesprins are membrane proteins of the outer nuclear membrane and connect the cytoskeleton via other binding-proteins with the

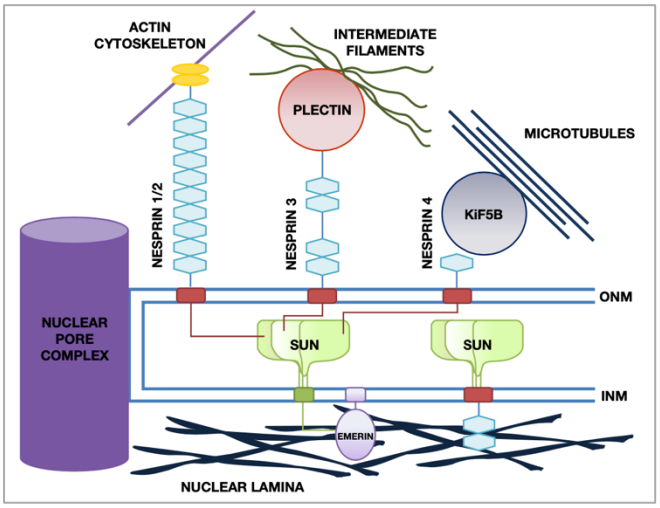


***Figure 2: The LINC complex:*** *Nesprin and sun proteins connect the cytoskeleton with the nucleoskeleton. Nesprins 1/2 interact with the actin filaments, nesprin-3 binds to intermediate filaments and nesprin-4 binds to microtubules. Sun proteins interact with the nuclear lamina and with nesprins in the perinuclear space (Rajgor and Shanahan 2013).*

nuclear envelope. The intermediate filaments bind to the protein nesprin-3 via the cytolinker plectin (Wilhelmsen, Litjens et al. 2005). Sun proteins are anchored to the inner nuclear membrane. They interact with the nuclear lamina and also with nesprin proteins in the perinuclear space between the inner and outer membrane (Starr and Fridolfsson 2010).

## 1.10 HYPOXIA

Cells are mainly cultured under atmospheric oxygen conditions (21 %), but this significantly differs from the oxygen concentrations in the tissue of living organisms. The mean oxygen concentration in adult human tissues is around 3 % (Csete 2005). In skeletal muscle tissue the oxygen level is approximately between 3 and 5 % (Bylund-Fellenius, Walker et al. 1981, Carreau, El Hafny-Rahbi et al. 2011, Beaudry, Hidalgo et al. 2016). Further, in exercising muscles the oxygen level is even lower, approximately 1 % (Bylund-Fellenius, Walker et al. 1981). In several studies the effect of hypoxia on myoblasts and myogenesis was investigated. It was shown that lower oxygen levels such as 3 % or 5 % do not affect myogenesis or proliferation rate but may even increase it (Chakravarthy, Spangenburg et al. 2001). Thus, 3 to 5 % of oxygen appears to be the optimum condition for proliferation and myogenesis of muscle cells (Beaudry, Hidalgo et al. 2016).

## 1.11 AIM OF THIS STUDY

The disease “desminopathy” is rare and currently there is no treatment option. Many pathological abnormalities of the disease still need further investigation. The aim of this study was to analyse the nuclear morphology of skeletal muscle-derived myoblasts with the complete absence of the intermediate filament protein desmin. Furthermore, the myoblasts were exposed to low oxygen concentrations to address the additional effect of more physiological growth conditions.

# 2 MATERIALS AND METHODS

## 2.1 MATERIALS

### *2.1.1 BUFFERS*

Lysis buffer

50 mM Tris/HCl pH 8.0
100 mM EDTA
100 mM NaCl
1 % SDS

TAE buffer (50x)

2 M Tris-Base
5.71 % Acetic acid
10 % 0.5 M EDTA pH 8.0
dd$H_2O$

TE buffer

1 M Tris/HCl pH 8.0
0.5 M EDTA
dd$H_2O$

### *2.1.2 ENZYMES*

| | |
|---|---|
| Proteinase K | Roth |
| 10x Trypsin diluted 1:10 in 1x PBS | Pan Biotech |

### *2.1.3 INHIBITORS*

| | |
|---|---|
| Trypsin Neutralizing Solution | Promocell |

### *2.1.4 MAMMALIAN CELL LINES*

Murine skeletal muscle-derived myoblasts, immortalized through p53 knock-out (Clemen & Berwanger, unpublished)

- myoblast line #88, musculus gastrocnemius, homozygous desmin knock-out
- myoblast line #121, Musculus gastrocnemius, wild-type

### *2.1.5 CELL CULTURE MEDIUM*

Growth Medium:

| | |
|---|---|
| Skeletal Muscle Cell Growth Medium | Promocell |
| + 5 % SupplementMix + 1 % Pen/Strep | |

Differentiation Medium:

| | |
|---|---|
| Dulbecco's Modified Eagle's Medium | Pan Biotech |
| + 5 % Horse Serum + 1 % Pyruvate + 1 % L-Glutamine | |
| + 1 % NEA + 1 % Pen/Strep | |

### *2.1.6 PCR-PRIMER*

| | | |
|---|---|---|
| DES 1 R | 5´-GGTCGTCTATCAGGTTGTCACG-3´ | metabion |
| DES 1 | 5´-TTGGGGTCGCTGCGGTCTAGCC-3´ | metabion |
| LacZ 430R | 5´-GATCGATCTCGCCATACAGCGC-3´ | metabion |

### *2.1.7 ANTIBODIES*

Primary antibodies:

| | |
|---|---|
| Rabbit anti-Desmin, polyclonal, #16520-1-AP | Proteintec |
| Rabbit anti-Emerin, polyclonal, #10351-1-AP | Proteintec |
| Mouse anti-Lamin A/C IgG2a, monoclonal, #4777 | Cell-Signaling |
| Rabbit anti-MACF1, polyclonal | Iakowos Karakesisoglou |
| Mouse anti-MyoD, monoclonal, #NB100-56511 | Novus Biologicals |
| Mouse anti-Nesprin-2 giant, monoclonal | Iakowos Karakesisoglou |
| Mouse anti-Pax7, monoclonal, #AB_528428 | DSHB |
| Mouse anti-α-actinin 2, monoclonal, #A7732 | Sigma-Aldrich |
| Mouse anti-γH2AX, monoclonal, #05-636 | Merck-Millipore |

Secondary antibodies:

| | |
|---|---|
| Fab fragment goat anti-mouse IgG, #115-007-003 (1:60) | Jackson ImmunoResearch |
| goat anti-mouse IgG, Alexa Fluor 405, #A-31553 | Thermo Fisher |
| donkey anti-goat IgG, Alexa Fluor 488, #A-11055 | Thermo Fisher |

| | |
|---|---|
| goat anti-mouse IgG1, Alexa Fluor 488, #A-21121 | Thermo Fisher |
| goat anti-mouse IgG, Alexa Fluor 568, #A-11004 | Thermo Fisher |
| goat anti-rabbit IgG, Alexa Fluor 568, #A-11011 | Thermo Fisher |
| goat anti-mouse IgG2a, Alexa Fluor 647, #A-21241 | Thermo Fisher |

#### *2.1.8 MISCELLANEOUS*

| | |
|---|---|
| Agarose | Promega |
| BSA | Sigma-Aldrich |
| DAPI | Roth |
| DMSO | Roth |
| dNTPs | Bio-Budget |
| Ethidium bromide | Roth |
| Gelatin | Sigma-Aldrich |
| Gelvatol/DABCO | Roth |
| Horse Serum (HS) | Pan Biotech |
| HyperLadder II | Bioline |
| Isopropanol | Roth |
| L-Glutamine | Pan Biotech |
| Mowiol + DABKO | Roth |
| NEA | Pan Biotech |
| PFA (4 %) | Alfa Aesar |
| Pyruvate | Pan Biotech |
| Red Taq 2x Master Mix | VWR |
| Triton X-100 | AppliChem |

### 2.2 METHODS

#### *2.2.1 COATING OF CELL CULTURE DISHES*

Since myoblasts do not adhere to uncoated cell culture dishes, the dishes were coated with gelatin. For this, 1 g gelatin was dissolved in 500 ml dd$H_2O$ and autoclaved for 20 min at 121°C. 3 ml of the 0.2 % gelatin solution was given on 100 mm dishes and 1 ml on the 35 mm micro-dishes (ibidi). The dishes were incubated for at least 1 h at 37°C and the remaining gelatin was removed immediately before use.

### 2.2.2 GENERATION OF MURINE MYOBLAST CELL LINES

Immortalized myoblast cell lines were previously generated by Clemen and Berwanger in 2017 (unpublished). Desmin knock-out mice (Li, Colucci-Guyon et al. 1996) were crossed with p53 knock-out mice (Jacks, Remington et al. 1994) and further mated to generate mice homozygous for both desmin and p53 knock-out as well as mice with the wild-type desmin allel in conjunction with the homozygous p53 knock-out. The mice were euthanized and the hind leg muscles (M. gastrocnemius and M. soleus) were dissected. From these muscles, satellite cells were obtained and cultured on gelatin-coated cell culture dishes. The resulting myoblasts were deep-frozen with DMSO via “MrFrostys” freezing container at -80°C and stored in a liquid nitrogen sample storage.

### 2.2.3 REVITALIZATION OF MYOBLASTS

For this study, two of the myoblast lines thus generated were used, homozygous desmin knock-out #88 and wild-type #121. Both cell lines were derived from Musculus gastrocnemius. After thawing the cryo-vials in a sterile workbench, the cells were transferred into tubes with 5 ml of Skeletal Muscle Cell Growth Medium (SMCG-medium, Promocell) and centrifuged at 500 x g for 8 min at RT. The supernatant was discarded, and the pellet was resuspended with 1x PBS. After that the tubes were again centrifuged (500 x g, 8 min, RT). The supernatant was again discarded, the pellets were resuspended with 5 ml of SMCG-medium and transferred on an uncoated 100 mm dish each. This step removes fibroblasts that contaminate the culture, because fibroblasts become quickly adherent on uncoated cell culture dishes. The dishes were incubated at 37 °C for 1 h. Afterwards the supernatants containing the myoblasts were transferred on 100 mm dishes coated with gelatin. The cells were incubated at 37 °C.

### 2.2.4 CULTIVATION OF MYOBLASTS

The myoblasts were daily checked under the light microscope (cf. figure 3). When the myoblasts had reached a confluence of approximately 70 %, the cells were splitted and distributed on new dishes. For this purpose, the medium was aspirated, and the cells were washed once with 2 – 3 ml 1x PBS. Then 1 ml trypsin was added and incubated at 37°C for 5 – 10 min to detach the myoblasts from the dishes. After that 1 ml trypsin neutralizing solution was added to stop the enzyme activity of trypsin. The solution with the cells was

transferred into a 15 ml tube. To remove remaining cells from the dishes, these were washed again with 1 – 5 ml 1x PBS and the solution was transferred into the tubes as before. The tubes were centrifuged at 500 x g for 8 min at RT. The supernatant was discarded, and the pellet was washed with 1x PBS. The tubes were centrifuged as before, and the supernatant was removed. The cell pellets were resuspended in 12 ml SMCG-medium, transferred on uncoated 100 mm dishes again to remove fibroblasts from the culture, and the cells were incubated at 37 °C for 1-2 h. After that, the supernatant with the myoblasts was transferred on 100 mm or 35 mm dishes coated with gelatin. For propagation, the cells were incubated at standard condition of 37°C and 5 % $CO_2$. Furthermore, the cells were cultivated at reduced oxygen levels as described below.

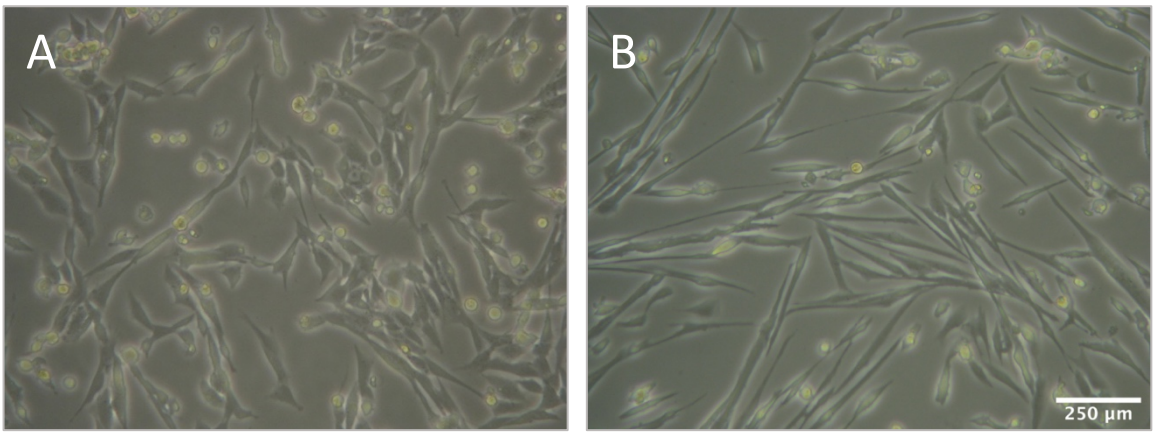


***Figure 3*** *Myoblasts four days after splitting.* ***A****: Desmin wild-type cell line #121 at passage 14.* ***B****: Homozygous desmin knock-out cell line #88 at passage 13.*

### *2.2.5 DIFFERENTIATION OF MYOBLASTS*

For differentiation of myoblasts into myotubes the SMCG-medium was replaced by Dulbecco's Modified Eagle's Medium (DMEM) supplemented with 5 % horse serum, 1 % pyruvate, 1 % L-glutamine, 1 % NEA and 1 % Pen/Strep. For 100 mm dishes 25 ml, for the smaller 35 mm dishes (ibidi) only 2 ml medium were added. The cells were differentiated for a time period of 5 to 6 days at 37°C and 5 % $CO_2$ and different oxygen concentrations as described below.

### 2.2.6 OXYGEN CONDITIONS

To study the effect of different oxygen levels on wild-type and homozygous desmin knock-out myoblasts and myotubes, they were cultivated at 21 % $O_2$ for "normoxia", 5 % $O_2$ for "physoxia" and 1 % $O_2$ for "physiological hypoxia" conditions in analogy to the oxygen levels determined in resting and exercising human skeletal muscle tissue (Bylund-Fellenius, Walker et al. 1981, Carreau, El Hafny-Rahbi et al. 2011, McKeown 2014, Beaudry, Hidalgo et al. 2016, Ast and Mootha 2019). Carbon dioxide and temperature were at standard conditions (5 % and 37°C).

Myoblasts grown or differentiated at reduced oxygen levels were neither splitted nor was medium changed or added. Since some proteins or signaling pathways within the cells adapt very quickly to changing $O_2$ conditions, the medium of the dishes cultured in lower oxygen levels were dumped out and the cells immediately fixed, i.e. the medium was not aspirated and the cells were not washed once with 1x PBS before fixation. To keep the conditions the same, this step was also not done for myoblasts grown at 21 % oxygen.

### 2.2.7 ISOLATION OF GENOMIC DNA

To isolate the genomic DNA (gDNA) of the myoblasts, a small pellet of the cells was transferred into a 1.5 ml tube. The pellet was lysed in 500 µl lysis mix and 25 µl proteinase K. The tubes were incubated at 55°C and 500 rpm overnight. After that the tubes were centrifuged at 16,000 x g for 5 min at RT. The supernatants were transferred into new 1.5 ml tubes, 500 µl isopropanol was added, and the tubes briefly inverted. After one hour of incubation at RT, the tubes were centrifuged at 4,000 x g for 10 min at RT and the supernatant was discarded. The pellets were washed once with 70 % ethanol and centrifuged again at 4,000 x g for 10 min at RT. Then the pellets were air-dried and solubilized in 100 µl TE buffer by incubating for 10 min at 65 °C (500 rpm) to dissolve the DNA. The tubes were further incubated at 4 °C overnight before using the gDNA for PCR analysis.

### 2.2.8 POLYMERASE CHAIN REACTION

The genotype of the myoblasts was controlled via polymerase chain reaction.

A standard reaction set up for desmin knock-out PCR was used:

10 µl Red Taq 2x Master Mix

0.4 µl primer forward DES 1

0.4 µl primer reverse DES1 R

0.4 µl primer LacZ 430R

2 µl template-DNA

ad 20 µl $ddH_2O$

Standard PCR program

| | | | |
|---|---|---|---|
| Step 1 (Denaturing) | 94°C | 4 min | |
| Step 2 (Denaturing) | 94°C | 1 min | n = 35 cycles |
| Step 3 (Annealing) | 62°C | 45 sec | |
| Step 4 (Extension) | 72°C | 1 min | |
| Step 5 (Completion) | 72°C | 5 min | |
| Step 6 4°C | for ever | | |

To analyse the PCR products, the samples were applied on a 1.5 % agarose gel for electrophoresis.

### *2.2.9 DNA AGAROSE GEL ELECTROPHORESIS*

To separate the DNA fragments in the samples, gel electrophoresis with 1.5 % agarose gels in 1x TAE buffer was performed. A horizontal electrophoresis tank was filled with 1x TAE buffer and 5 µl of ethidium bromide. To evaluate the size of the DNA fragments, the DNA-size marker HyperLadder II was loaded next to the samples. The gel was run at 220 V for 45 min and finally documented with Alpha Innotec gel documentation system with UV light illumination. The expected sizes of the products were 350 bp for wild-type cells and 450 bp for homozygous desmin knock-out cells. Heterozygous samples would show both bands.

### *2.2.10 CELL SAMPLES FOR IMMUNFLUORESCENCE MICROSCOPY*

For immunofluorescence analysis, cells were grown in 35 mm micro-dishes with plastic coverslips at the bottom suitable for microscopy (ibidi). The cells were transferred to these

smaller dishes during the splitting process and incubated in reduced or standard oxygen conditions.

To fix the cells for immunofluorescence stainings, the medium in the micro-dishes was removed, 400 µl of 4 % paraformaldehyde was added and incubated for 20 min at RT. After that, the dishes were washed twice with 1x PBS and 2 ml of 1x PBS were added to prevent the samples from drying out. The cells were then stored at 4°C until the staining was performed.

### *2.2.11 IMMUNOFLUORESCENCE STAINING*

The fixed cells stored at 4 °C were washed three times with 1x PBS. The cells were permeabilized for 30 min at RT with 0.5 % Triton X-100 in PBS and washed three times with 1x PBS afterwards. Residual formaldehyde was blocked with 0.15 % glycine in 1x PBS for 10 min at RT. Again, the cells were washed three times for 5 min with 1x PBS. To block non-specific binding sites the cells were incubated with 1 % BSA in PBS for 1 h at RT. After three washing steps with 1x PBS (5 min each), the first primary antibody, diluted in 0.5 % BSA with 0.1 % Triton X-100 in PBS, was incubated at 4°C in humid chambers overnight. At the next day, the compatible secondary antibody (diluted 1:400 in 0.5 % BSA with 0.1 % Triton X-100 in PBS) was added and incubated for 1 h at RT in the dark. These steps were repeated several times with different primary and secondary antibodies until 2 to 4 different stainings were applied (see staining protocol below). Every primary antibody was incubated overnight at 4°C and every secondary antibody was incubated for 1 h at RT. The Fab fragment goat anti-mouse IgG (diluted 1:60 in 0.5 % BSA with 0.1 % Triton X-100 in PBS) used to “convert” the species of one of the primary antibodies was also incubated for 1 h at RT, and DAPI was stained with the last secondary antibody. After each antibody the cells were washed 6 times with 1x PBS for 5 min. Finally, the micro-dishes were briefly rinsed with $ddH_2O$ and the cells were embedded in Gelvatol/DABCO or Mowiol/DABCO. The myoblasts were covered with glass coverslips and cured at RT overnight. To prevent samples from fading, all working steps with fluorescence-labelled antibodies were protected from light and completed dishes were stored in the dark at 4°C.

The following combinations of antibody stainings were performed:

1. 1st Ab: Pax7 (mouse mAb, IgG1, 1:100, 3,19µg/mL) + MyoD (mouse mAb, IgG1, 1:200), 2nd Ab: goat anti-mouse IgG1 Alexa 488
   3rd Ab: Emerin (rabbit pAb, 1:75, Proteintec), 4th Ab: goat anti-rabbit Alexa 568
   3rd Ab: Lamin A/C (mouse mAb, IgG2a, 1:200, Cell Signaling), 4th Ab: goat anti-mouse IgG2a Alexa 647
   DAPI (1mg/mL in Methanol, 1:1000)

2. 1st Ab: Pax7 (mouse mAb, IgG1, 1:100, 3,19µg/mL) + MyoD (mouse mAb, IgG1, 1:200), 2nd Ab: goat anti-mouse IgG1 Alexa 488
   3rd Ab: Desmin (rabbit pAb, 1:100, Proteintec), 4th Ab: goat anti-rabbit Alexa 568
   3rd Ab: Lamin A/C (mouse mAb, IgG2a, 1:200, Cell Signaling), 4th Ab: goat anti-mouse IgG2a Alexa 647
   DAPI (1mg/mL in Methanol, 1:1000)

3. 1st Ab: Pax7 (mouse mAb, IgG1, 1:100, 3,19µg/mL) + MyoD (mouse mAb, IgG1, 1:200), 2nd Ab: goat anti-mouse IgG1 Alexa 488
   3rd Ab: Nesprin-3 27132-1-AP (rabbit pAb, 1:100), 4th Ab: goat anti-rabbit Alexa 568
   3rd Ab: Lamin A/C (mouse mAb, IgG2a, 1:200, Cell Signaling), 4th Ab: goat anti-mouse IgG2a Alexa 647
   DAPI (1mg/mL in Methanol, 1:1000)

4. 1st Ab: Pax7 (mouse mAb, IgG1, 1:100, 3,19µg/mL) + MyoD (mouse mAb, IgG1, 1:200), 2nd Ab: goat anti-mouse IgG1 Alexa 488
   3rd Ab: MACF1 (rabbit pAb, 1:200), 4th Ab: goat anti-rabbit Alexa 568
   3rd Ab: Lamin A/C (mouse mAb, IgG2a, 1:200, Cell Signaling), 4th Ab: goat anti-mouse IgG2a Alexa 647
   DAPI (1mg/mL in Methanol, 1:1000)

5. 1st Ab: Pax7 (mouse mAb, 1:100, 3,19µg/mL) + MyoD (mouse mAb, 1:200), 2nd Ab: Fab goat anti-mouse, 3rd Ab: donkey anti-goat Alexa 488
   4th Ab: Nesprin-2 giant (mouse mAb, 1:5), 5th Ab: goat anti-mouse Alexa 568
   DAPI (1mg/mL in Methanol, 1:1000)

6. 1st Ab: Pax7 (mouse mAb, 1:100, 3,19µg/mL) + MyoD (mouse mAb, 1:200), 2nd Ab: Fab goat anti-mouse, 3rd Ab: donkey anti-goat Alexa 488
   4th Ab: γH2AX (mouse mAb, IgG1, 1:500), 5th Ab: goat anti-mouse Alexa 405
   6th Ab: Emerin (rabbit pAb, 1:75, Proteintec), 7th Ab: goat anti-rabbit Alexa 568
   6th Ab: Lamin A/C (mouse mAb, IgG2a, 1:200, Cell Signaling), 7th Ab: goat anti-mouse IgG2a Alexa 647
   w/o DAPI

Secondary antibody stainings as negative controls:

1. 1st Ab: Fab goat anti-mouse, 2nd Ab: donkey anti-goat Alexa 488
   2nd Ab: goat anti-rabbit Alexa 568

2. 1st Ab: goat anti-mouse Alexa 405
   1st Ab: goat anti-mouse IgG1 Alexa 488
   1st Ab: goat anti-mouse Alexa 568
   1st Ab: goat anti-mouse IgG2a Alexa 647

### *2.2.12 MICROSCOPY*

Immunofluorescence microscopic images were recorded using a TCS SP5 confocal laser scanning microscope equipped with HyD detectors (Leica, software LAS AF version 2.73.9723) with an HCX PL APO 63x/1.40 oil immersion objective followed by image deconvolution using Hygens Essential (Jan 2016; Scientific Volume Imaging B.V., deconvolution conducted by Prof. Dr. Christoph Clemen).

### *2.2.13 TIME LAPSE MOVIES WITH JuLI™ Br*

Time lapse movies were recorded using a compact light microscope, Live Cell Analyzer JuLI Br (NanoEnTek), placed in the cell culture incubator. With this device cell proliferation and cellular fusion into myotubes was monitored. Time lapse movies of myoblasts and myotube development were recorded for the different oxygen conditions. The standard set up was 4x magnification and one picture every 2 min for myoblasts proliferation for a period of time between 2 - 3 days and every 10 min for myotube formation for a period of 5 to 6 days for analysis of myotube differentiation. Myoblast confluence was determined with the Ju-Li™ Br PC software.

### *2.2.14 DETERMINATION OF NUCLEAR SHAPE*

The sizes of the major and minor axes of the (mostly) ovoid myoblast nuclei, marked with the Lamina A/C antibody, were manually determined using the LAS AF Lite offline software (Leica). The data was transmitted to MS excel. Furthermore, the morphology of the nuclei was categorized into normal or abnormal with respect to an essentially smooth or an irregular/folded nuclear lamina, respectively.

### *2.2.15 MEASURING THE NUMBER OF γH2AX SPOTS*

To detect DNA damages within the nuclei, the myoblasts were marked with the γH2AX antibody (cf. 4.2.11 IMMUNOFLUORESCENCE STAINING). γH2AX is a histone phosphorylation, that marks double-strand breaks in the nucleus for repair (Mah, El-Osta et al. 2010). The antibody visualizes DNA damages as spots, called foci. The number of foci within the nuclei were automatically counted using the programme ImageJ.

### *2.2.16 MUSCLE TISSUE SLICES*

In a similar study conducted by a student member of a cooperating work group (details to be published elsewhere), skeletal muscle tissue sections derived from wild-type and homozygous desmin knock-out mice were stained with a hematoxylin and eosin staining, which stains nuclei blue and cytoplasm red (Wang, Yue et al. 2017). The images were then digitalized and an AI algorithm was employed to recognize nuclei and measure their area. This data was used for comparison to the results of this study.

### *2.2.17 STATISTICAL ANALYSES*

The data of nuclear axes and DNA damage were checked for nominal distribution using the Shapiro-Wilk test. For this nonparametric data a Kruskal-Wallis one-way analysis of variance was performed to test differences between groups. For comparison of two distinct groups, Mann-Whitney-Wilcoxon rank-sum tests were performed. Nominal data was tested via Fisher's exact test (2x2 and 2x4 contingency tables). The significance limit was set at 0.05 for all tests. MS Excel and RStudio were used for graphical presentation.

# 3 RESULTS

## 3.1 GENOTYPING

On order to verify the genotype of the myoblast lines, samples were subjected to PCR genotyping. A representative result of the PCR and the gel electrophoresis is shown in figure 4. A band of approximately 350 bp was obtained for myoblast line #121, confirming the cells as desmin wild-type (wt). The 450 bp band of myoblast line #88 verified the cells as homozygous desmin knock-out (hom). Therefore, the myoblasts were expanded and used for the subsequent analyses.

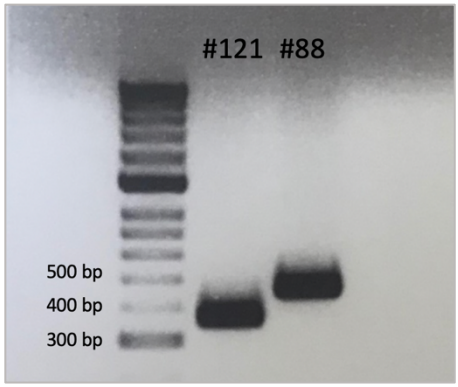


***Figure 4:*** *Agarose gel image to determine the genotypes of the cell lines #88 and #121.*

## 3.2 MYOBLAST GROWTH

For a basic characterization of the cell lines, growth curves were recorded using a compact live cell microscope placed in the incubator. This device monitored the confluence of the myoblast cultures for a period of 48 h as shown in figure 5.

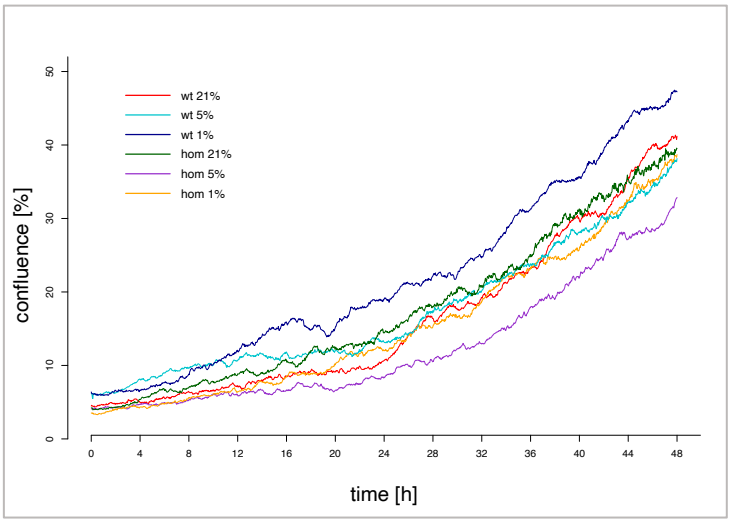


***Figure 5****: Confluence of the wild-type and homozygous desmin knock-out myoblasts at different oxygen conditions in 48 h. Recording was started immediately after cell splitting.*

For all cell culture dishes the start confluence was adjusted to 3 to 6 %. The exact start and final confluences are given in Table 1.

The curves of wild-type (wt) and homozygous desmin knock-out (hom) myoblasts at 21 % oxygen were almost identical, reaching final confluences of 41 and 39 %, respectively. At 5 % oxygen, the wild-type cells grew a little bit slower than at 21 %, they started with a confluence of approximately 6 % but ended with a confluence of only about 38 %. This was the lowest confluence of wild-type cells of all three oxygen conditions. The homozygous desmin knock-out cells also showed the lowest growth at 5 % oxygen, with a confluence of

only 32 % after 48 h. At 1% oxygen, the curve of the homozygous DKO myoblasts was again similar to the curve at 21% oxygen, while the wild-type cells showed a greater confluence with over 47%.

***Table 1:*** *The confluences of the myoblasts at the beginning and end of the recordings at different oxygen concentrations.*

| | confluency [%] | | | |
|---|---|---|---|---|
| | wt | | hom | |
| oxygen conc. | 0 h | 48 h | 0 h | 48 h |
| 21% | 4,47 | 41,19 | 4,22 | 39,49 |
| 5% | 6,23 | 38,16 | 4,07 | 32,87 |
| 1% | 6,39 | 47,23 | 3,53 | 38,70 |

## 3.3 MYOBLAST DIFFERENTIATION

To evaluate the myogenic potential of the myoblasts, time lapse movies of the myotube development were recorded. In all oxygen conditions the myoblasts were able to fuse into myotubes. However, the homozygous desmin knock-out myoblasts differentiated faster than the wild-type cells as illustrated in figure 6. The number of resulting myotubes of homozygous cells was larger and these myotubes were markedly thicker. Moreover, it was observed, that wild-type myotubes more frequently detached from the culture dish surface, and became visible as cell lumps in the light microscope images (cf. figure 6: A). Further, it was noted that wild-type myotubes started to spontaneously contract after a differentiation time of approximately 6 days. This was rarely noticeable in the homozygous desmin knock-out cells. Finally, wild-type and the homozygous desmin knock-out myotubes were used for a first set of immunofluorescence stainings with an $\alpha$-actinin-2 antibody (figure 6: C,D), which marks the Z-bands in the sarcomeres (Ribeiro Ede, Pinotsis et al. 2014). While this characteristic striated pattern was visible in the wild-type myotubes, homozygous desmin knock-out myotubes typically showed an incomplete $\alpha$-actinin signal pattern (figure 6: C, D).

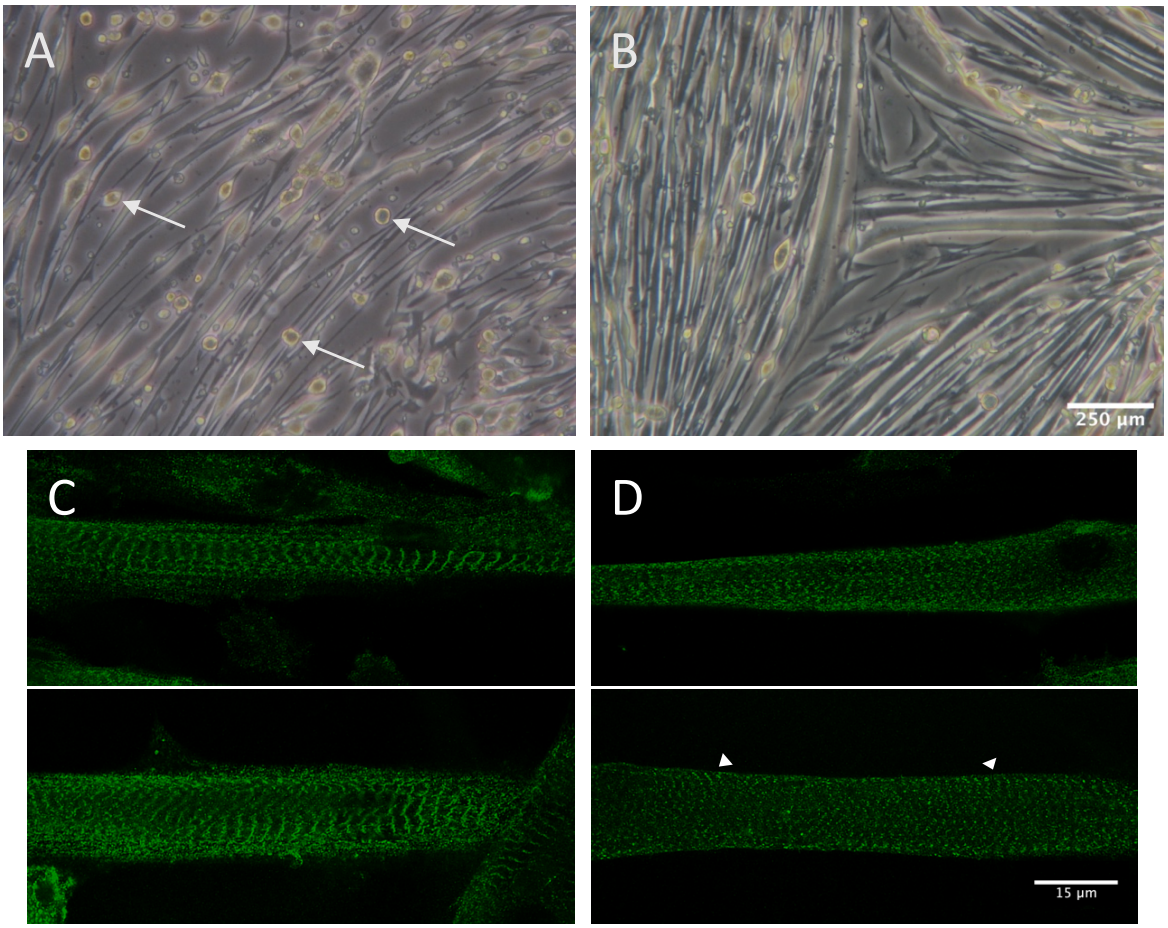


***Figure 6:*** *Representative light (**A, B**) and immunofluorescence microscope (**C, D**) images of myotubes at 21 % oxygen. **A**: Wild-type at day 6 of differentiation. Myotubes are thin and partially have detached from the surface and are visible as lumps (arrows). **B**: Homozygous desmin knock-out myotubes at day 6 of differentiation. The myotubes are thicker. **C, D**: Myotubes stained with an α-actinin-2 antibody. **C:** Wild-type myotubes showed the typical cross-striated pattern. **D**: Myotubes of homozygous desmin knock-out myoblasts were less well differentiated with the α-actinin-2 signal being more incomplete (arrowheads).*

## 3.4 IMMUNOFLUORESCENCE STAININGS

To have a closer look on the morphology of the myoblast nuclei, various immunofluorescence stainings were performed to visualize the nuclear envelope or the nuclear lamina. Therefore, proteins from the LINC complex were immunostained, i.e., emerin, lamin A/C, nesprin-2 giant, and nesprin-3. The best signal quality was obtained from the lamin A/C staining, so the length of the major and minor axes of nuclei was measured based on these images, as well as the categorization in abnormally or normally shaped nuclei.

To differentiate myoblasts from existing fibroblast contaminations in the cultures, Pax7 and MyoD, both muscular transcription factors, were stained alone or in combination. However, their nuclear staining turned out to be highly variable with respect to the signal intensity and the ratio between Pax7 and MyoD-positive nuclei. This situation could not be

improved by different passages of the myoblasts, cell fixation with formaldehyde or methanol, various antibody concentrations, and different immunofluorescence staining protocols either. Therefore, contaminating fibroblasts could only be identified by their light microscopic cell morphology. Desmin immunostaining in wild-type cells was positive in approximately 70 % of the cells and showed the typical desmin filament network (see figure 8). Desmin negative cells were mostly immature myoblasts, which did not yet express desmin.

Due to time limitations for optimizing some of the stainings and additional technical problems of the laser scanning microscope, not all preparations were imaged (e.g. myoblasts, exposed to an oxygen concentration of 5 %). However, images of successful test stainings as well as secondary antibody control can be found in the appendix section (p.38).

### *3.4.1 NUCLEAR MORPHOLOGY*

To analyse the nuclear shape and size of wild-type and homozygous myoblasts 1,037 nuclei were counted and measured.

The nuclear shape of the wild-type and the homozygous cells were mostly ovoid to round. Some of the myoblasts showed nuclear abnormalities in form of a grooved or crumpled nucleus. In homozygous cells, a higher number of abnormal nuclei was present. It was noticeable that cells growing in higher density seem to have more often abnormalities in shape than in lower density. Therefore, myoblast preparations grown at a similar low cell confluence were used for the analyses.

Wild-type myoblasts, grown at 21 % oxygen showed a significant smaller number of abnormal nuclei than homozygous desmin knock-out myoblasts ($p \approx 2.4x10^{-26}$). The relative frequency was 24.63 % for wild-type and 68.03 % for homozygous myoblasts (cf. table 2). Homozygous desmin knock-out myoblasts exposed to 1 % oxygen showed a significant decrease compared to homozygous myoblasts exposed to 21 % oxygen ($p \approx 5.5x10^{-12}$). Only 38.46 % of the nuclei had noticeable abnormalities. Notably, no significant effect of oxygen concentration on nuclei of wild-type cells was observed ($p \approx 0.915$). The relative frequency was 24.07 %, similar to the value for 21 % oxygen. The number of abnormal nuclei of homozygous desmin knock-out myoblasts at 1% oxygen was still significantly higher than the number of abnormal wild-type nuclei at an oxygen concentration of 1% and 21% ($p \approx 0.001$ and $p \approx 0.001$).

***Table 2**: Absolut and relative number of abnormal DKO myoblast nuclei at different oxygen levels.*

| | Number of abnormal nuclei | | | |
|---|---|---|---|---|
| | wt | | hom | |
| oxygen level | absolute | relative [%] | absolute | relative [%] |
| 21% | 66 | 24.63 | 217 | 68.03 |
| 1% | 52 | 24.07 | 90 | 38.46 |

A difference in nuclear size between wild-type and homozygous desmin knock-out myoblasts was also detected. A comparison of the average length of the nuclei axes is shown in table 3. Homozygous nuclei appeared significantly smaller than those of the wild-type. The major and minor axes of the nuclei of wild-type myoblasts were significantly longer than those of the homozygous desmin knock-out myoblasts when exposed to 21 % oxygen ($p \approx 3.25 \times 10^{-34}$ and $p \approx 3.93 \times 10^{-41}$). Nuclei of myoblasts exposed to 1 % oxygen showed a significant increase in the length of major and minor axes. But the major and minor axes of wild-type nuclei were still significantly longer than those of the homozygous cells ($p \approx 5.56 \times 10^{-24}$ and $p \approx 1.39 \times 10^{-30}$). A visualization of the data is shown in figure 7, representative immunofluorescence images are given in figure 8.

***Table 3**: Average length of major and minor axes of myoblast nuclei at different oxygen levels.*

| | average length of axes | | | |
|---|---|---|---|---|
| | wt | | hom | |
| oxygen level | major [µm] | minor [µm] | major [µm] | minor [µm] |
| 21% | 14.2709 | 10.7754 | 11.7220 | 7.9783 |
| 1% | 15.0889 | 11.2246 | 12.9412 | 8.6965 |

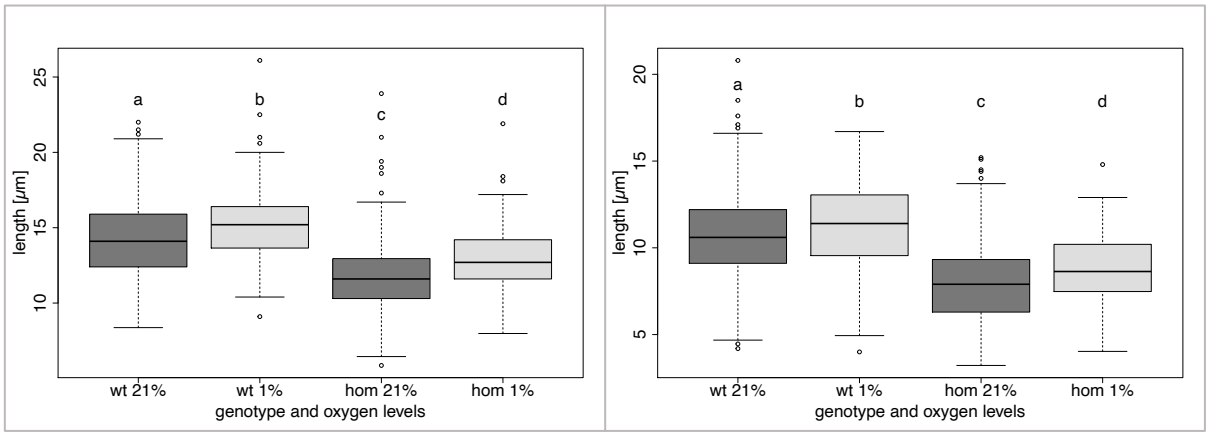


***Figure 7:** Boxplots of the lengths of the major axis (left) and minor axis (right) of the myoblast nuclei. Different letters above the plots show statistically significant differences as indicated in the text.*

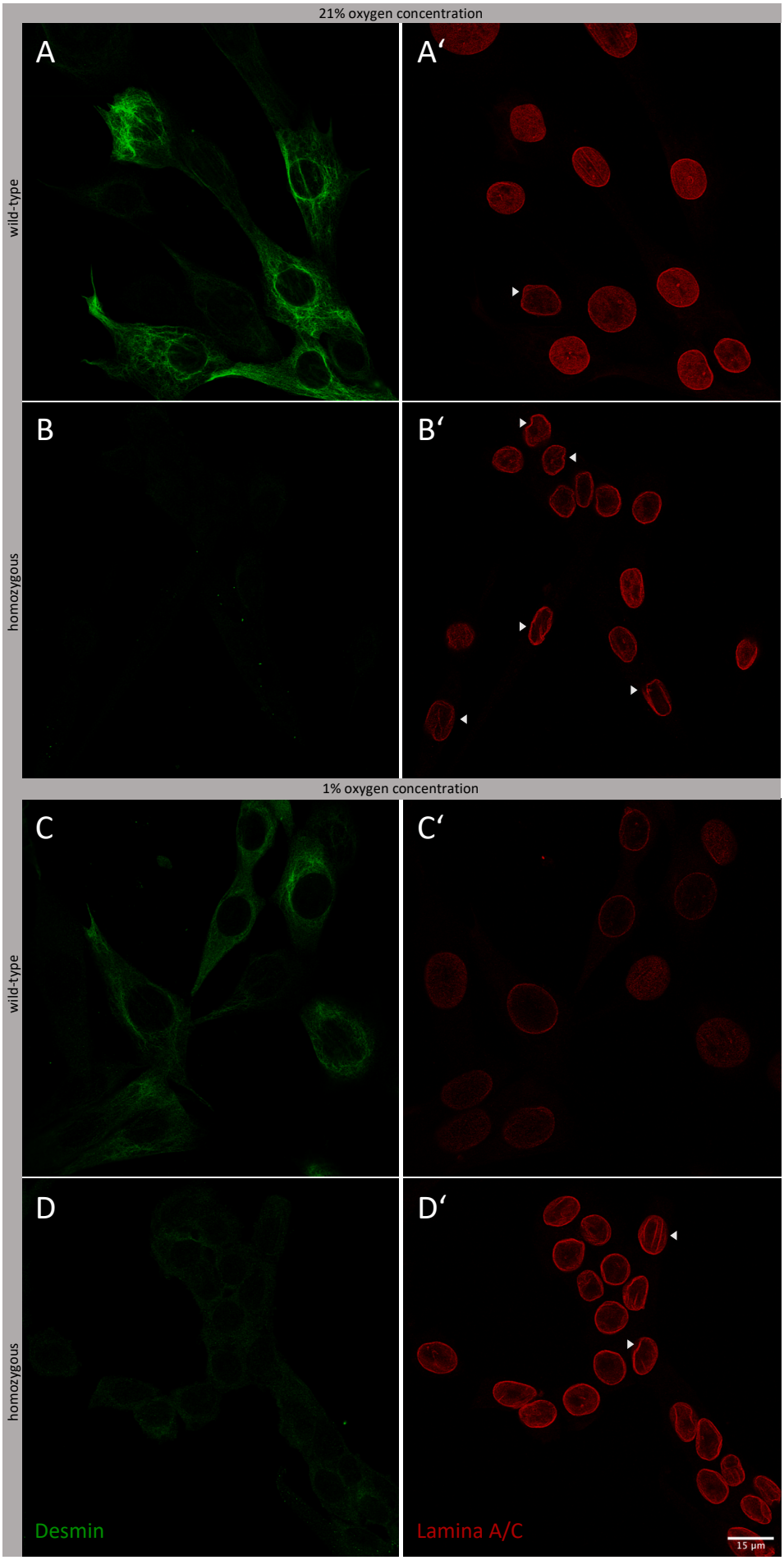


***Figure 8**: Representative confocal images of the myoblasts at different oxygen concentrations. The desmin cytoskeleton network **(A-D)** and the nuclear lamina **(A'-D')** were stained. Abnormal nuclear shapes are marked (arrowheads).*

### 3.4.2 DNA DAMAGE

A γH2AX staining was used to visualize DNA damages in form of double-strand breaks (Mah, El-Osta et al. 2010). The average number of γH2AX-positive foci is presented in figure 9. Despite the rather high dispersion of values, the Kruskal-Wallis test showed a p-value of about 1.13x10^-17.

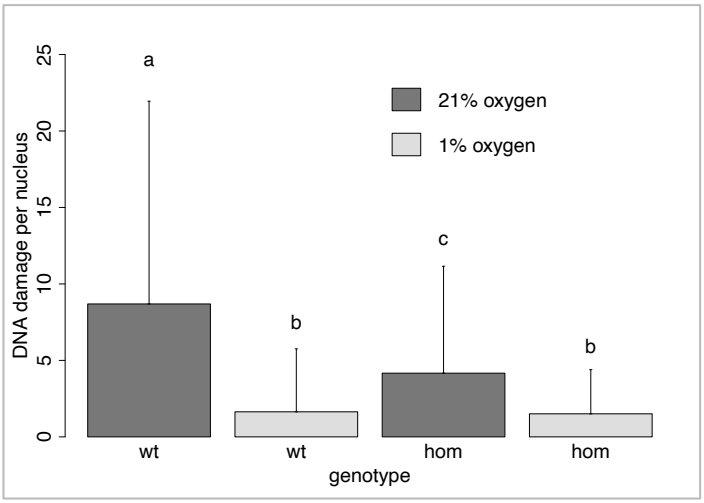


***Figure 9:*** *Average number of γH2AX-positive foci representing DNA damage of myoblasts per nucleus. Different letters above the bars indicate statistically significant differences. Error bars show the standard deviation.*

The average number of γH2AX-positive foci per nucleus for wild-type myoblasts at 21 % oxygen concentration was approximately 9. Homozygous myoblasts had a significant lower average of about 4 foci (p≈0.003). A significant decrease was observed at an oxygen concentration of 1 % with only about 1 γH2AX-positive focus per nucleus in both genotypes (p≈0.167 for wild-type vs. homozygous myoblasts at 1 % oxygen). Representative images of the staining are shown in figure 10.

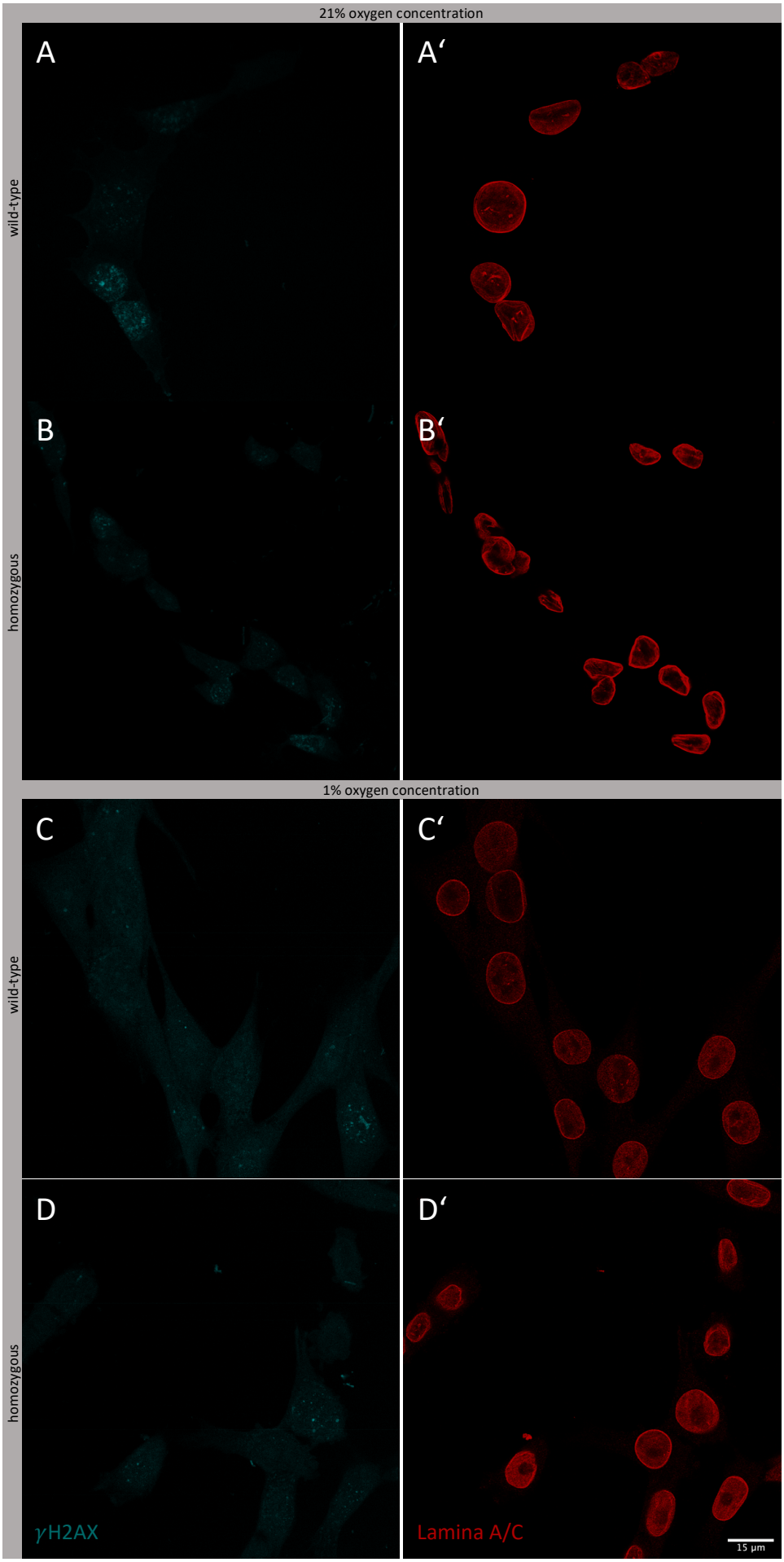


***Figure 10:*** *Representative confocal images of myoblasts at different oxygen levels. Double-strand breaks were marked with an γH2AX antibody (**A-D**) and the corresponding nuclei marked with a lamin A/C antibody (**A'-D'**). Note the abnormal nuclear shape of homozygous myoblasts.*

# 4 DISCUSSION

## 4.1 MYOBLAST GROWTH and DIFFERENTIATION

The confluences of wild-type and desmin knock-out myoblasts differed only slightly in the first 48 hours after the splitting process. However, small differences were noticed when the cells were exposed to lower oxygen concentrations. Our findings suggest that an oxygen concentration of 1 % or 21 % does not affect the growth of homozygous myoblasts, while 5 % oxygen has an inhibitory effect. In wild type cells, on the other hand, 1% has a rather beneficial effect, while 5% also has a mild inhibitory effect. The small inhibitory effect of an oxygen concentration of 5 % is not consistent with the findings of Chakravarthy et al. (2001) or Beaudry et. al. (2016), who discribed that a lower oxygen concentration of 3 to 5 % increases proliferation or that this concentration could be a optimal condition. In a study of Ren, Accili et al. (2010) an oxygen concentration of 1 % also led to an increase in proliferation. However, it should be noted that our data are based on one time-lapse video each. Further analyses have to be performed to confirm the findings, either by additional time-lapse videos or by manual counting using a Neubauer's chamber.

Both cell lines were able to differentiate into multinucleated myotubes (cf. figure 6). Based on the light microscopy images (cf. figure 6), it is noticeable that the desmin knock-out myoblasts differentiated faster and formed larger myotubes. Thus, the absence of desmin does not affect the successful development of myoblasts into myotubes. This was also observed in homozygous desmin knock-out mice that did not show conspicuous defects in muscle development, but developed myopathies only during their lifetime (Li, Colucci-Guyon et al. 1996). However, the homozygous desmin knock-out myotubes showed a disordered cross-striation pattern, which underlines that desmin is needed for a correct alignment of the myofibrils within the myotubes (Clemen, Herrmann et al. 2013).
The observed detachment of mostly wild-type myotubes from the dishes can be caused by their spontaneous contractions.

## 4.2 NUCLEAR MORPHOLOGY

The differences of the nuclear shape of wild-type and homozygous desmin knock-out myoblasts were significant. In general, the ovoid or round nuclei of myoblasts differed from the more spindle-shaped nuclei of cardiac muscle cells, but skeletal muscle myoblasts also

showed the crumpled or grooved nuclear envelope, which were described in the study by Heffler et al. (2020). The reason for these invaginations has not yet been addressed in detail, but it could be an effect of the missing connection of the desmin filament to the LINC complex (Heffler, Shah et al. 2020). Since it has been reported that nuclear shape has influence on gene expression (Skinner and Johnson 2017), the defect in nuclear shape in form of the observed grooved or crumpled nuclear envelope in desmin knock-out myoblasts may also have such an effect.

The serious consequences that defects in the LINC complex or associated proteins can have, become apparent in patients with Hutchinson-Gilford progeria syndrome. This disease is caused by a mutation of lamin A, which is part of the nuclear lamina and e.g binding partner of the sun proteins of the LINC complex (Vidak and Foisner 2016). Lobulated or crumpled nuclei can also be observed in progeria patients (Goldman, Shumaker et al. 2004).

The decrease of nuclear abnormalities at lower oxygen concentration were rather unexpected. In neurons, which however are very sensitive to low oxygen levels, it was observed that nuclei swell during hypoxia as a sign of injury (Dehghani, Karatas et al. 2018). As the nucleus swells, the nuclear envelope may become smoother. The size of the myoblast nuclei actually increased at an oxygen concentration of 1%, but it is unlikely that this is also an indication of injury of the myoblasts, since this is approximately the physiological oxygen concentration of an exercising muscle (Bylund-Fellenius, Walker et al. 1981). Also, both myoblast lines were able to proliferate and differentiate when exposed to 1 % oxygen. The confluence of wild-type cells even increased during the low oxygen level. Thus, the reason for a decrease of the number of abnormally shaped nuclei of homozygous desmin knock-out myoblasts at lower oxygen concentration remains unknown for now and has to be further investigated.

## 4.3 NUCELAR SIZE

Nuclei of homozygous desmin knock-out myoblasts were in general smaller than the wild-type nuclei. In yeasts a smaller cell size led to a smaller nuclear size (Huber and Gerace 2007). Though the size of the homozygous myoblasts was not measured, it appeared to be smaller compared to the wild-type cells. It is also known that a high Pax7 expression leads to smaller cells (Collins, Gnocchi et al. 2009). In this respect, in some of the immunofluorescence stainings, the homozygous myoblasts showed a higher proportion of Pax7 and

MyoD positive nuclei than the wild-type. Smaller nuclear sizes were also observed in desmin knock-downs of cardiomyocytes (Heffler, Shah et al. 2020).

Statistically significant smaller nuclei were also determined in skeletal muscle tissue slices derived from homozygous desmin knock-out mice in comparison to the wild-type littermates (see Material and Methods, paragraph 2.2.16; not part of this work). The myonuclei of homozygous desmin knock-out mice showed a mean nuclear area of 19.1 µm$^2$ compared to 20.3 µm$^2$ in the wild-type mice ($p \approx 1.72x10\text{^}-23$, approximately 20,000 nuclei were measured). This demonstrates that our data obtained from cultured, immortalized myoblasts are also consistent with data in mature muscle tissue.

## 4.4 DNA DAMAGE

It is proven that hypoxia reduces the repair of double-strand breaks by homologous recombination (Chan, Koritzinsky et al. 2008, Kumareswaran, Ludkovski et al. 2012), but the cells used in these studies were exposed to very low oxygen levels of 0.02 %. In our study the opposite effect was detected; the number of $\gamma$H2AX-positive foci per nucleus was markedly decreased, when myoblasts were exposed to 1 % oxygen. It should be noted, that a 1 % oxygen concentration is more physiological to myoblasts and exercising muscle can have an even lower oxygen concentration (Bylund-Fellenius, Walker et al. 1981). That differs to other tissues, where oxygen concentration lies about 1-10 % (Carreau, El Hafny-Rahbi et al. 2011). There could be basically different DNA damage repair processes in myoblasts.

Furthermore, the probability of forming harmful radical oxygen species is increased at higher oxygen concentrations (Hemnani and Parihar 1998). This can also be a reason for the higher number of $\gamma$H2AX-positive foci per nucleus observed, when myoblasts were exposed to 21 % oxygen. However, it remains unclear, why the wild-type myoblasts showed more foci than the homozygous myoblasts. It cannot be entirely excluded that other defects have manifested in the used cells lines due to mutations. Since reactive oxygen species are byproducts of metabolism (Forrester, Kikuchi et al. 2018), there could also be an imbalance. In fact, defects in the mitochondria have been detected in homozygous desmin knock-out mice (unpublished, not part of this work), which might possibly lead to less reactive oxygen species and therefore to less foci. In contrast, a desmin knock-down in cardiomyocytes showed a higher number of $\gamma$H2AX-positive foci than their control. It was assumed that the abnormal nuclear shape was responsible for this observation (Heffler, Shah

et al. 2020). However, this cannot be concluded from our data, since the desmin knock-out cells showed markedly less $\gamma$H2AX-positive foci.

### 4.5 ERROR ANALYSIS

For an alternative distinction of myoblasts and fibroblasts, one could have used an additional staining of vimentin. Like desmin, it is an intermediate filament protein that is expressed in fibroblasts, but limited to the early development of myoblasts (Sax, Farrel et al. 1989). Several of the performed immunofluorescence stainings showed no signal or high background levels and must be further optimized. A reduction of the stainings to 1 to 2 per ibidi could possibly lead to an improvement.

## 5 CONCLUSION and OUTLOOK

The nuclei of desmin knock-out myoblasts showed crumpled or grooved shapes, smaller size and a reduced number of $\gamma$H2AX-positive foci. At lower oxygen concentration a partial decrease in wild-type and homozygous desmin knock-out myoblasts could be observed. To what extent this nuclear shape and size influences the clinical picture of recessive desminopathies remains unclear und must be further investigated.

Next, our findings of the immunofluorescence images should be proven by western blotting. Thus, could be tested if our myoblasts were stressed by the lower oxygen levels of 5 and 1 % by analyzing the presence of Hif1$\alpha$, a transcription factor, expressed when cells are exposed to hypoxia (Li, Zhu et al. 2007). In addition, the already immunostained myoblasts preparation grown at an oxygen concentration of 5 % must be imaged and analyzed. Furthermore, the myotubes differentiated at lower oxygen concentration must be imaged as well. Based on these images, the nuclei can also be examined for abnormalities, size as well as successful positioning in the periphery of the myotube. It would be interesting, if homozygous DKO myotubes show displaced nuclei, because of the missing connection of desmin to the LINC complex. Moreover, a comparison must also be made with the findings in skeletal muscle tissue.

# 6 REFERENCES

Abe, T., K. Takano, A. Suzuki, Y. Shimada, M. Inagaki, N. Sato, T. Obinata and T. Endo (2004). "Myocyte differentiation generates nuclear invaginations traversed by myofibrils associating with sarcomeric protein mRNAs." J Cell Sci **117**(Pt 26): 6523-6534.

Ast, T. and V. K. Mootha (2019). "Oxygen and mammalian cell culture: are we repeating the experiment of Dr. Ox?" Nature Metabolism **1**(9): 858-860.

Beaudry, M., M. Hidalgo, T. Launay, V. Bello and T. Darribere (2016). "Regulation of myogenesis by environmental hypoxia." J Cell Sci **129**(15): 2887-2896.

Boujard, D., B. Anselme, C. Cullin and C. Raguénès-Nicol (2014). Zell- und Molekularbiologie im Überblick, Springer-Verlag Berlin Heidelberg.

Bylund-Fellenius, A.-C., P. M. Walker, A. Elander, S. Holm, J. Holm and T. Schersten (1981). "Energy metablosim in relation to oxygen partial pressure in human skeletal muscle during exercise." Biochem. J. **200**(2): 247-255.

Carreau, A., B. El Hafny-Rahbi, A. Matejuk, C. Grillon and C. Kieda (2011). "Why is the partial oxygen pressure of human tissues a crucial parameter? Small molecules and hypoxia." J Cell Mol Med **15**(6): 1239-1253.

Cartwright, S. and I. Karakesisoglou (2014). "Nesprins in health and disease." Semin Cell Dev Biol **29**: 169-179.

Chakravarthy, M. V., E. E. Spangenburg and F. W. Booth (2001). "Culture in low levels of oxygen enhances in vitro prolifer- ation potential of satellite cells from old skeletal muscles." CMLS Cellular and Molecular Life Sciences **58**(8): 1150-1158.

Chal, J. and O. Pourquie (2017). "Making muscle: skeletal myogenesis in vivo and in vitro." Development **144**(12): 2104-2122.

Chan, N., M. Koritzinsky, H. Zhao, R. Bindra, P. M. Glazer, S. Powell, A. Belmaaza, B. Wouters and R. G. Bristow (2008). "Chronic hypoxia decreases synthesis of homologous recombination proteins to offset chemoresistance and radioresistance." Cancer Res **68**(2): 605-614.

Christen, P., R. Jaussi and R. Benoit (2016). Cytoskelett und molekulare Motoren. Biochemie und Molekularbiologie**:** 297-304.

Clemen, C. S., H. Herrmann, S. V. Strelkov and R. Schröder (2013). "Desminopathies: pathology and mechanisms." Acta Neuropathol **125**: 47-75.

Collins, C. A., V. F. Gnocchi, R. B. White, L. Boldrin, A. Perez-Ruiz, F. Relaix, J. E. Morgan and P. S. Zammit (2009). "Integrated functions of Pax3 and Pax7 in the regulation of proliferation, cell size and myogenic differentiation." PLoS One **4**(2): e4475.

Csete, M. (2005). "Oxygen in the cultivation of stem cells." Ann N Y Acad Sci **1049**: 1-8.

Dehghani, A., H. Karatas, A. Can, E. Erdemli, M. Yemisci, E. Eren-Kocak and T. Dalkara (2018). "Nuclear expansion and pore opening are instant signs of neuronal hypoxia and can identify poorly fixed brains." Sci Rep **8**(1): 14770.

Forrester, S. J., D. S. Kikuchi, M. S. Hernandes, Q. Xu and K. K. Griendling (2018). "Reactive Oxygen Species in Metabolic and Inflammatory Signaling." Circ Res **122**(6): 877-902.

Goldman, R. D., D. K. Shumaker, M. R. Erdos, M. Eriksson, A. E. Goldman, L. B. Gordon, Y. Gruenbaum, S. Khuon, M. Mendez, R. Varga and F. S. Collins (2004). "Accumulation of mutant lamin A causes progressive changes in nuclear architecture in Hutchinson-Gilford progeria syndrome." Proc Natl Acad Sci U S A **101**(24): 8963-8968.

Gros, J., M. Manceau, V. Thome and C. Marcelle (2005). "A common somitic origin for embryonic muscle progenitors and satellite cells." Nature **435**(7044): 954-958.

Heffler, J., P. P. Shah, P. Robison, S. Phyo, K. Veliz, K. Uchida, A. Bogush, J. Rhoades, R. Jain and B. L. Prosser (2020). "A Balance Between Intermediate Filaments and Microtubules Maintains Nuclear Architecture in the Cardiomyocyte." Circulation Research **126**(3): 10-26.

Hemnani, T. and M. S. Parihar (1998). "Reactive oxygen sprecies and oxydative DNA damage." Indian J Physiol Pharmacol **42**(4): 440-452.

Henderson, M., L. De Waele, J. Hudson, M. Eagle, C. Sewry, J. Marsh, R. Charlton, L. He, E. L. Blakely, I. Horrocks, W. Stewart, R. W. Taylor, C. Longman, K. Bushby and R. Barresi (2013). "Recessive desmin-null muscular dystrophy with central nuclei and mitochondrial abnormalities." Acta Neuropathol **125**(6): 917-919.

Herrmann, H., H. Bar, L. Kreplak, S. V. Strelkov and U. Aebi (2007). "Intermediate filaments: from cell architecture to nanomechanics." Nat Rev Mol Cell Biol **8**(7): 562-573.

Herrmann, H., S. V. Strelkov, P. Burkhard and U. Aebi (2009). "Intermediate filaments: primary determinants of cell architecture and plasticity." J Clin Invest **119**(7): 1772-1783.

Hetzer, M. W. (2010). "The nuclear envelope." Cold Spring Harb Perspect Biol **2**(3): a000539.

Hnia, K., C. Ramspacher, J. Vermot and J. Laporte (2015). "Desmin in muscle and associated diseases: beyond the structural function." Cell Tissue Res **360**(3): 591-608.

Hoffmann, K., K. Sperling, A. L. Olins and D. E. Olins (2007). "The granulocyte nucleus and lamin B receptor: avoiding the ovoid." Chromosoma **116**(3): 227-235.

Huber, M. D. and L. Gerace (2007). "The size-wise nucleus: nuclear volume control in eukaryotes." J Cell Biol **179**(4): 583-584.

Jacks, T., L. Remington, B. Williams, E. Schmitt, S. Halachmi, R. Bronson and R. Weinberg (1994). "Tumor spectrum analysis in p53-mutant mice." Curr Biol **4**(1): 1-7.

Kassar-Duchossoy, L., B. Gayraud-Morel, D. Gomes, D. Rocancourt, M. Buckingham, V. Shinin and S. Tajbakhsh (2004). "Mrf4 determines skeletal muscle identity in Myf5:Myod double-mutant mice." Nature **431**(7007): 466-471.

Kumareswaran, R., O. Ludkovski, A. Meng, J. Sykes, M. Pintilie and R. G. Bristow (2012). "Chronic hypoxia compromises repair of DNA double-strand breaks to drive genetic instability." J Cell Sci **125**(Pt 1): 189-199.

Li, X., L. Zhu, X. Chen and M. Fan (2007). "Effects of hypoxia on proliferation and differentiation of myoblasts." Med Hypotheses **69**(3): 629-636.

Li, Z., E. Colucci-Guyon, M. Pincon-Raymond, M. Mericskay, S. Pournin, D. Paulin and C. Babinet (1996). "Cardiovascular Lesion and Skeletal Myopathy in Mice Lacking Desmin." Developmental Biology **175**(2): 362-366.

Li, Z., A. Lilienbaum, G. Butler-Browne and D. Paulin (1989). "Human desmin-coding gene: complete nucleotide sequence, characterization and regulation of expression during myogenesis and development." Gene **78**: 243-254.

Mah, L. J., A. El-Osta and T. C. Karagiannis (2010). "gammaH2AX: a sensitive molecular marker of DNA damage and repair." Leukemia **24**(4): 679-686.

McKeown, S. R. (2014). "Defining normoxia, physoxia and hypoxia in tumours-implications for treatment response." Br J Radiol **87**(1035): 20130676.

Milner, D. J., G. E. Taffet, X. Wang, T. Pham, T. Tamura, C. Hartley, A. M. Gerdes and A. M. Capetanaki (1999). "The Absence of Desmin Leads to Cardiomyocyte Hypertrophy and Cardiac Dilation with Compromised Systolic Function." J Mol Cell Cardiol **31**: 2063–2076.

Milner, D. J., G. Weitzer, D. Tran, A. Bradley and Y. Capetanaki (1996). " Disruption of Muscle Architecture and Myocardial
Degenerationin Mice Lacking Desmin." J Cell Biol **134**(5): 1255-1270.

Ott, M.-O., G. Lyons, H. Arnold and M. Buckingham (1991). "Early expression of the myogenic regulatory gene, myf-5, in precursor cells of skeletal muscle in the mouse embryo." Development **111**(4): 1097-1107.

Rajgor, D. and C. M. Shanahan (2013). "Nesprins: from the nuclear envelope and beyond." Expert Rev Mol Med **15**: e5.

Relaix, F., D. Rocancourt, A. Mansouri and M. Buckingham (2005). "A Pax3/Pax7-dependent population of skeletal muscle progenitor cells." Nature **435**(7044): 948-953.

Ren, H., D. Accili and C. Duan (2010). "Hypoxia converts the myogenic action of insulin-like growth factors into mitogenic action by differentially regulating multiple signaling pathways." Proc Natl Acad Sci U S A **107**(13): 5857-5862.

Ribeiro Ede, A., Jr., N. Pinotsis, A. Ghisleni, A. Salmazo, P. V. Konarev, J. Kostan, B. Sjoblom, C. Schreiner, A. A. Polyansky, E. A. Gkougkoulia, M. R. Holt, F. L. Aachmann, B. Zagrovic, E. Bordignon, K. F. Pirker, D. I. Svergun, M. Gautel and K. Djinovic-Carugo (2014). "The structure and regulation of human muscle alpha-actinin." Cell **159**(6): 1447-1460.

Ruppert, T., M. B. Heckmann, K. Rapti, D. Schultheis, A. Jungmann, H. A. Katus, L. Winter, N. Frey, C. S. Clemen, R. Schroder and O. J. Muller (2020). "AAV-mediated cardiac gene transfer of wild-type desmin in mouse models for recessive desminopathies." Gene Ther.

Sax, C. M., F. X. Farrel and Z. E. Zehner (1989). "Down-regulation of vimentin gene expression during myogenesis is controlled by a 5'4lanking sequence." Gene **78**: 235-242.

Schröder, R. and B. Schoser (2009). "Myofibrillar Myopathies: A Clinical and Myopathological Guide." Brain Pathology **19**(3): 483-492.

Skinner, B. M. and E. E. Johnson (2017). "Nuclear morphologies: their diversity and functional relevance." Chromosoma **126**(2): 195-212.

Starr, D. A. and H. N. Fridolfsson (2010). "Interactions between nuclei and the cytoskeleton are mediated by SUN-KASH nuclear-envelope bridges." Annu Rev Cell Dev Biol **26**: 421-444.

van Spaendonck-Zwarts, K. Y., L. van Hessem, J. D. Jongbloed, H. E. de Walle, Y. Capetanaki, A. J. van der Kooi, I. M. van Langen, M. P. van den Berg and J. P. van Tintelen (2011). "Desmin-related myopathy." Clin Genet **80**(4): 354-366.

Vidak, S. and R. Foisner (2016). "Molecular insights into the premature aging disease progeria." Histochem Cell Biol **145**(4): 401-417.

Wang, C., F. Yue and S. Kuang (2017). "Muscle Histology Characterization Using H&E Staining and Muscle Fiber Type Classification Using Immunofluorescence Staining." Bio Protoc **7**(10).

Wilhelmsen, K., S. H. Litjens, I. Kuikman, N. Tshimbalanga, H. Janssen, I. van den Bout, K. Raymond and A. Sonnenberg (2005). "Nesprin-3, a novel outer nuclear membrane protein, associates with the cytoskeletal linker protein plectin." J Cell Biol **171**(5): 799-810.

Wright, W. E., D. A. Sassoon and V. K. Lin (1989). "Myogenin, a Factor Regulating Myogenesis, Has a Domain Homologous to MyoD." Cell Press **56**(4): 607-617.

# 7 APPENDIX

## 7.1 REPRESENTATIVE IMMUNOFLUORESCENCE IMAGE OF NEGATIVE CONTROL

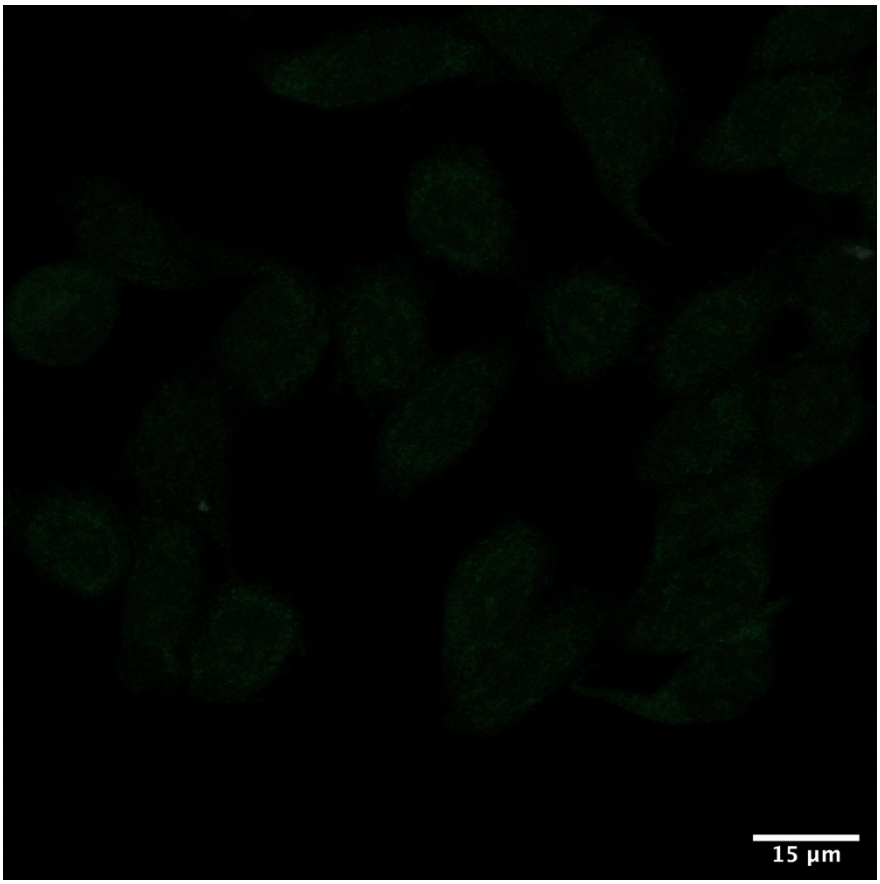


***Figure 11:*** *Overlay image of the negative control of the immunofluorescence staining with only secondary antibodies. Antibodies: goat anti-mouse Alexa 405, goat anti-mouse IgG1 Alexa 488, goat anti-mouse Alexa 568 and goat anti-mouse IgG2a Alexa 64. Small cell staining is noticeable but unspecific and of very low intensity.*

## 7.2 IMMUNOFLUORESCENCE TEST STAININGS

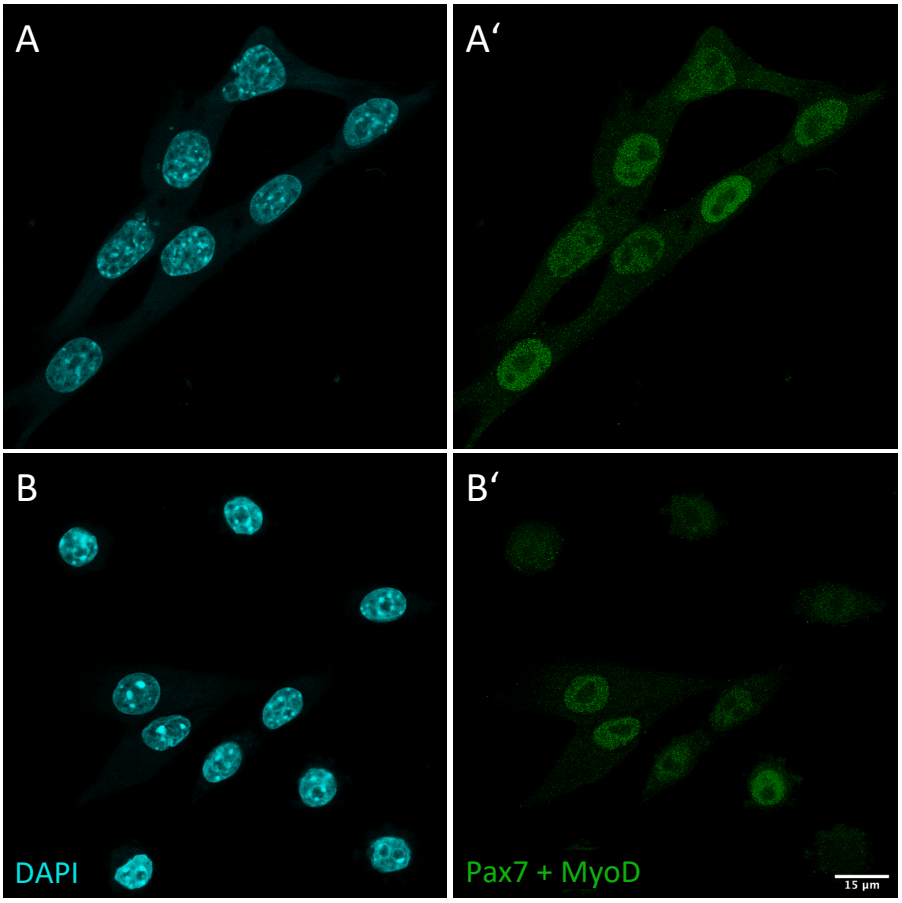


***Figure 12:*** *Representative images of the combined Pax7+ MyoD staining during a test staining. The upper images show DKO wild-type myoblasts stained with DAPI (**A**) and with a Pax7/MyoD antibody combination (**A’**). The lower images show the homozygous desmin knock-out myoblasts. Again, nuclei stained with DAPI (**B**) and a Pax7/MyoD antibody combination (**B’**).*

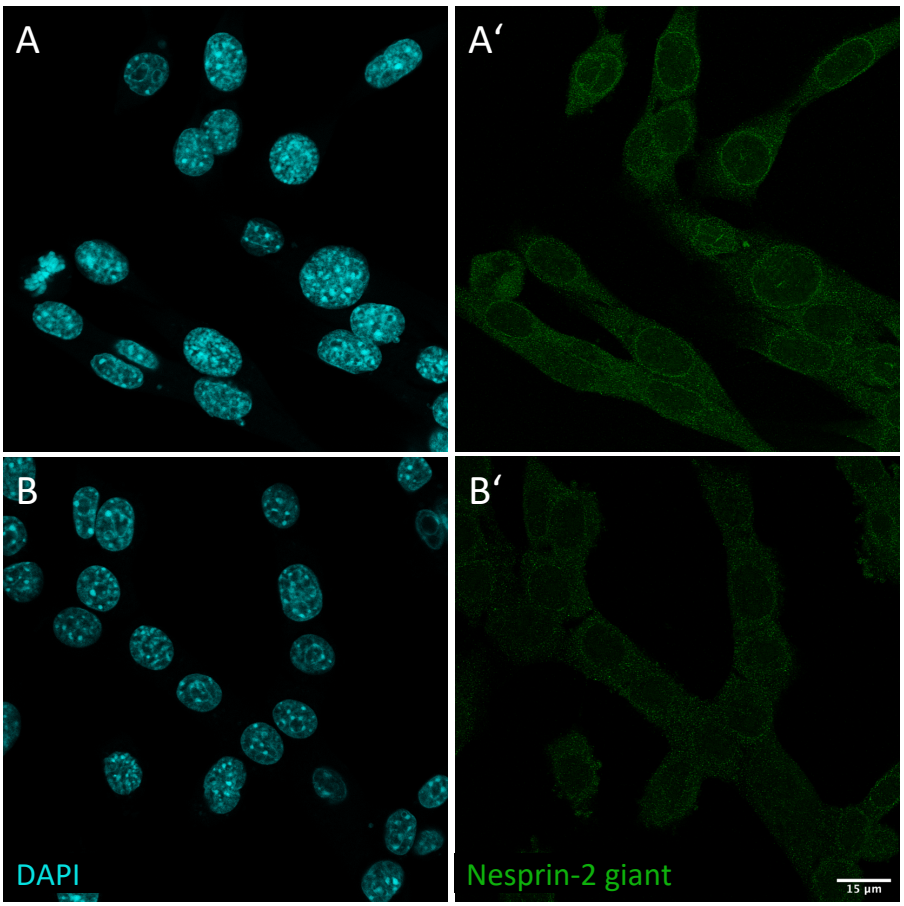


***Figure 13****: Representative images of the nesprin-2 giant (nuclear envelope) staining during a test staining (21 % oxygen). The upper images show DKO wild-type myoblasts stained with DAPI (**A**) and with a nesprin-2 giant antibody (**A’**). The lower images show the homozygous desmin knock-out myoblasts again nuclei stained with DAPI (**B**) and with a nesprin-2 giant antibody (**B’**). Note the weaker staining of nesprin-2 giant of the homozygous nuclei.*